ChemComm

Chemical Communications

www.rsc.org/chemcomm

Number 42 | 14 November 2008 | Pages 5245–5440

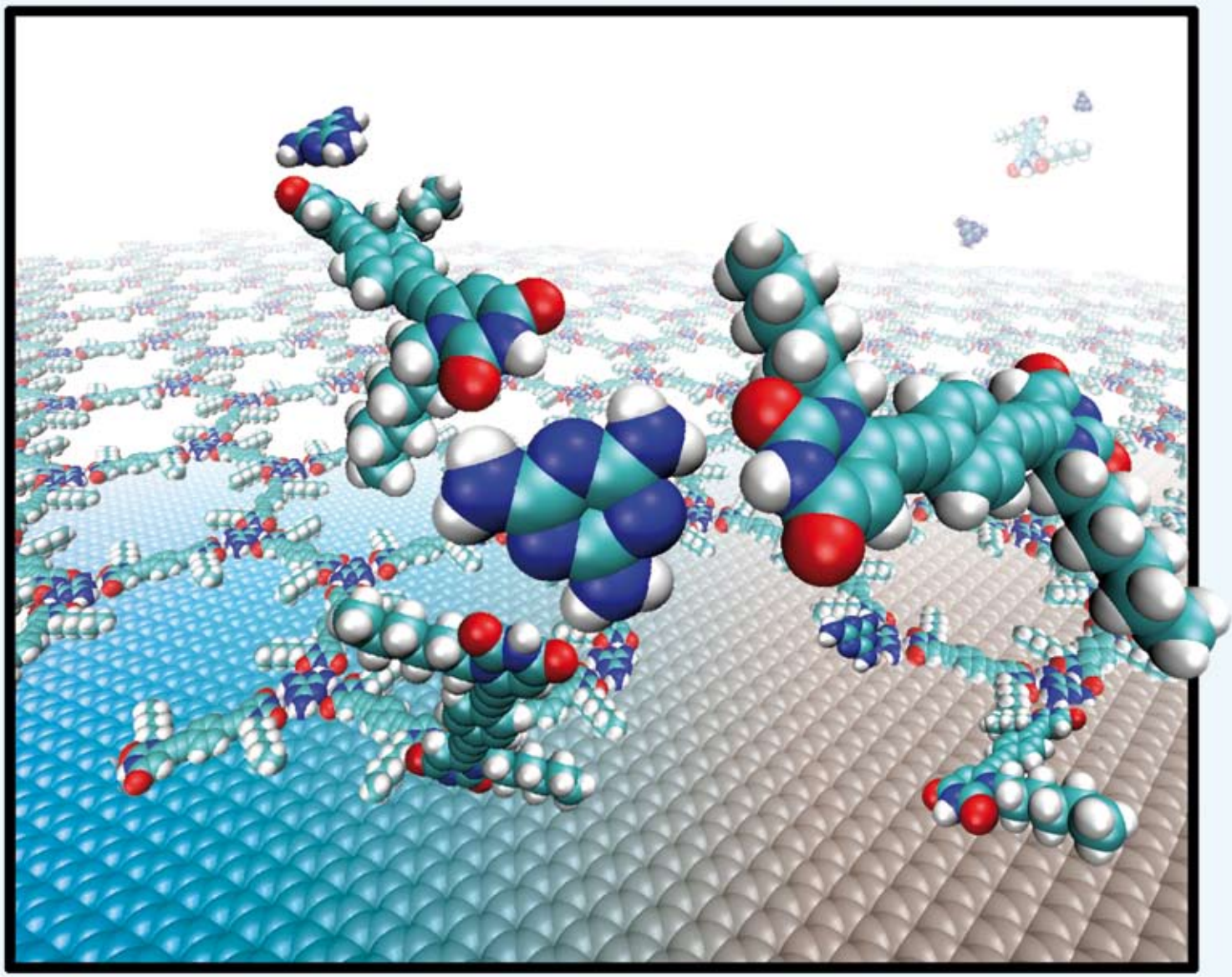

ISSN 1359-7345

RSC Publishing

1359-7345(2008)42;1-Z

Pre-programmed bicomponent porous networks at the solid–liquid interface: the low concentration regime†

Carlos-Andres Palma,[a] Massimo Bonini,*[b] Anna Llanes-Pallas,[c] Thomas Breiner,[b] Maurizio Prato,[c] Davide Bonifazi*[cd] and Paolo Samorí*[ae]

Received (in Cambridge, UK) 7th July 2008, Accepted 28th July 2008
First published as an Advance Article on the web 18th September 2008
DOI: 10.1039/b811534f

The control over the formation of a bicomponent porous network was attained by self-assembly at the solid–liquid interface, exploiting triple H-bonds between melamine and bis-uracyl modules.

While three-dimensional (3D) crystal engineering is a well-established field,[1] in the past few years there has been an increasing effort towards the fabrication of two-dimensional (2D) patterns.[2–4] In particular, the need for engineering of functional materials with sub-nanometre precision has triggered research on the development of perfectly ordered architectures exploiting weak yet highly directional interactions, such as metal–ligand or H-bonding.[4] Alongside the efforts devoted to self-assembled architectures under ultra-high vacuum (UHV) conditions,[3,4] the use of the crystal engineering approaches at the solid–liquid interface has also rapidly expanded due to their versatility: ordered architectures can be assembled by mixing the molecular building blocks and controlling their concentration.[5,6] In this respect, scanning tunneling microscopy (STM) operating both at the solid–liquid interface[2] and under UHV,[3,4] enables the nanoscale characterization of these supramolecular 2D architectures offering a detailed insight into the structures at the sub-molecular level. Despite these efforts, complete control over the formation of multi-component architectures at the solid–liquid interface has been not yet achieved.

Melamine, with its three-fold symmetry, represents a suitable system for engineering multidimensional H-bonded architectures both in solution and in the solid state.[7] Recently such a module, mixed with perylene tetracarboxylic di-imide (PTCDI), has been used to form highly ordered 2D arrays on Ag/Si(111) as thoroughly characterized by STM in an UHV at room temperature (rt).[8]

Herein, we report for the first time on the use of melamine (**2**) to direct the generation of bicomponent H-bonded networks at the solid–liquid interface. In particular, hexagonal porous networks have been tailored through the co-deposition of solutions containing melamine (**2**) and a bis-functionalized uracyl-bearing linear module (**1**)[9] (Scheme 1) on highly oriented pyrolitic graphite (HOPG) surfaces. Additionally, detailed STM experiments allowed the semi-quantitative determination of those energetic parameters essential for promoting the formation of porous structures over tightly packed monolayers, thus offering a reliable prediction of the formation of 2D assemblies at the solid–liquid interface.

STM images of mono-component self-assembled arrays obtained by depositing solutions of molecular modules **1** (29 ± 19 μM) and **2** (40 ± 25 μM) in 1,2,4-trichlorobenzene (TCB) on HOPG surfaces are displayed in Fig. 1a and b, respectively.[6] Both systems form highly crystalline monolayers. In the lower part of Fig. 1a, the contrast in the STM image reveals three bright lobes coinciding with the three aligned aromatic rings of molecule **1**. The hexyl side-chains not being physisorbed on surface, van der Waals interactions are predominantly occurring between the aromatic cores. The unit cell amounts to $a = 0.87 \pm 0.03$ nm, $b = 1.79 \pm 0.08$ nm and $\alpha = 65 \pm 1^\circ$ with an area (A) of 1.4 ± 0.2 nm^2. As expected, melamine (**2**) forms a hexagonal pattern with unit cell $a = 1.1 \pm 0.1$ nm, $b = 1.0 \pm 0.2$ nm, $\alpha = 61 \pm 3^\circ$ and

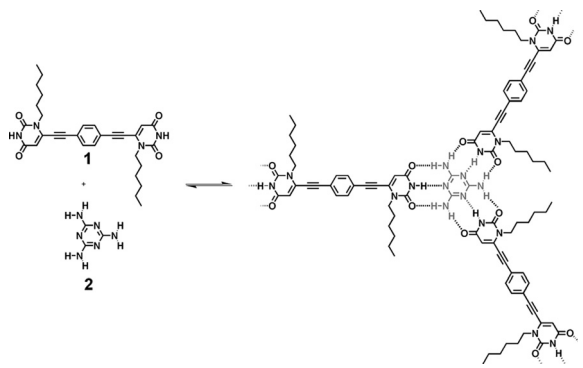

Scheme 1 The molecular structures of the investigated molecular modules **1** and **2**. The formation of the hybrid $\{[(\mathbf{1})_3{\cdot}(\mathbf{2})_2]_n\}$ assembly through intermolecular H-bonds at the solid–liquid interface is also depicted.

[a] *Nanochemistry Laboratory, ISIS/CNRS 7006, Université Louis Pasteur, 8 allée Gaspard Monge, 67000 Strasbourg, France. E-mail: samori@isis-ulp.org*
[b] *BASF SE, GKD/I, 67056 Ludwigshafen, Germany. E-mail: m.bonini@isis-ulp.org*
[c] *Università degli Studi di Trieste, Dipartimento di Scienze Farmaceutiche and INSTM UdR di Trieste, Piazzale Europa 1, 34127 Trieste, Italy*
[d] *University of Namur, Department of Chemistry, Rue de Bruxelles 61, 5000 Namur, Belgium. E-mail: davide.bonifazi@fundp.ac.be*
[e] *Istituto per la Sintesi Organica e la Fotoreattività, Consiglio Nazionale delle Ricerche, via Gobetti 101, 40129 Bologna, Italy*

† Electronic supplementary information (ESI) available: Experimental details for STM experiments; STM images of porous network showing the evolution in a 1D array, the porous network showing two hexagons linked by a 1D chain, and the tightly packed self-assembled monolayer of module **1**. See DOI: 10.1039/b811534f

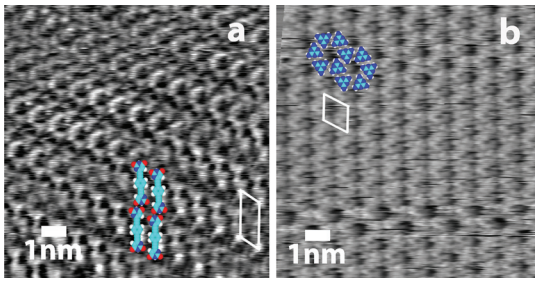

Fig. 1 STM height images of the mono-component assembly of (a) **1** and (b) **2** on HOPG. Alkyl chains are not shown in the model. (a) Average tunnelling current (I_t) = 16 pA and bias voltage (V_t) = 400 mV; (b) I_t = 15 pA and V_t = −400 mV.

$A = 0.9 \pm 0.1$ nm^2, in very good agreement with that observed under UHV conditions.[10]

The two aforementioned solutions have been mixed and diluted with TCB to yield concentrations of 3 ± 2 μM and 2 ± 1 μM of **1** and **2**, respectively. By applying 5 μL of this new solution to the HOPG surface, a porous network has been obtained at the solid–liquid interface, as visualized by *in situ* STM imaging at rt (Fig. 2). The unit cell parameters are $a = 3.9 \pm 0.2$ nm, $b = 3.9 \pm 0.2$ nm, $\alpha = 60 \pm 3°$ and $A = 13.4 \pm 0.6$ nm^2. Fig. 2b shows a close-up of the ordered assembly, evidence of the presence of hexagonal pores. Although we cannot resolve at the sub-molecular level both components in the images, the shape and size of the hexagonal pores are in perfect agreement with the models depicted in Fig. 2d. However, the combination of these two compounds at the graphite–TCB interface also leads to the generation of other polygonal pores ranging from pentagons to octagons (Fig. 2a). This can be explained taking into account the geometrical flexibility brought into play by the H-bonding interactions. In particular, a deviation of −8° or +12° from the ideal value of 120° for the angle **1–2–1** is sufficient to

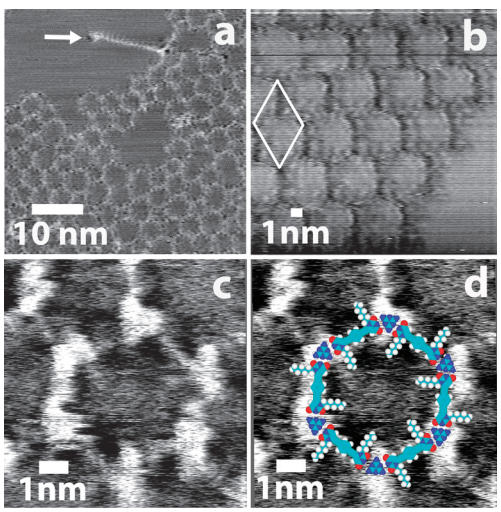

Fig. 2 STM height images of the self-assembled $\{[(\mathbf{1})_3{\cdot}(\mathbf{2})_2]_n\}$ pattern. (a) Polygonal structure, an arrow indicates the formation of a 1D assembly. (b) A close-up of an ordered hexagonal assembly. (c) Detail of a supramolecular hexagon and (d) the proposed assembly model. (a) I_t = 5 pA and V_t = 400 mV; (b) I_t = 30 pA and V_t = −600 mV; (c, d) I_t = 0.5 pA and V_t = −500 mV.

generate heptagons or pentagons, respectively. Yet it is not clear if the distribution of the different geometrical shapes is stochastic or phenomenological. The arrow in Fig. 2a indicates a linear structure germinating from an edge of a polygon. Given that these types of architectures have always been found to nucleate from a melamine edge (Fig. S1†) and that they resemble the arrays of molecule **1** at the same magnification (Fig. S2†), we can ascribe such a structure to a supramolecular assembly composed of molecules **1** linearly arranged through homo-coupling H-bonds. Time-resolved evidence of the growth of such a 1D array is shown in Fig. S3†, proving a high dynamic nature of these bicomponent porous networks.

It is worth noting that porous networks have not been observed on films prepared using concentrated solutions, *i.e.* having a concentration higher than 20 μM. Due to the emergence of competitive physisorption between modules **1** and **2** at the solid–liquid interface, at high concentrations only melamine molecules were found to be physisorbed on HOPG because of its high interaction energy per unit area (see below). In fact, the observed porous architectures displayed in Fig. 2 have been obtained with rather diluted solutions, *i.e.* featuring a sub-monolayer coverage. For instance, taking into account the pattern's unit cell of assembly $[(\mathbf{1})_3{\cdot}(\mathbf{2})_2]$ featuring an area $A = 13.4 \pm 0.6$ nm^2, which consists of three molecules of **1** and two molecules of **2**, a full monolayer on 1 cm^2 of a flat HOPG substrate contains in total 61 pmol of molecules **1** and **2** (Table 1). If we assume a complete physisorption over 1 cm^2, under our experimental conditions, *i.e.* 5 μL of a ~2 μM **1**–**2** solution physisorbed on HOPG, there are *ca.* three times fewer molecules than those required to fully cover the surface with a self-assembled monolayer. By assuming a sub-monolayer coverage and a complete physisorption of the components at the interface, the prediction of the most stable network is simplified since the number of molecules on HOPG is constant. Moreover, under such conditions, the physisorption *vs.* solvation equilibrium is very strongly shifted towards the former, thus the supernatant solution can be disregarded. Under these circumstances, we can thus describe and predict the formation and stability of the observed assemblies by using the same method employed to interpret the assembly behavior of PTCDI and melamine under UHV-STM.[8] The prediction of the molecular packing is not described by the minimization of the free interface energy per unit area, but rather by the total energy of the pattern consisting of N adsorbed molecules and the anisotropic–isotropic intermolecular interactions.[8] In the present work we extend this approach to the prediction of supramolecular assemblies at the solid–liquid interface in the low concentration regime. Under our working conditions, we have a fixed number of molecules, all of them physisorbed at the surface. Thus we can consider that: (i) the molecule–solvent interactions are negligible and (ii) the solvent–substrate interactions do not govern the pattern formation, although they can further stabilize the 2D assembly. In view of this, we can apply a previously devised approach which considers the molecule–molecule interactions as the only contribution driving the pattern formation at the surface.

Table 1 semi-quantitatively illustrates this principle. The porous network formation is predicted if the concentration

Table 1 Calculated energies for the formation of a monolayer on HOPG neglecting the molecule–solvent and solvent–substrate interactions. C_S = surface concentration in a monolayer over an ideally flat HOPG surface; E_H = energy per H-bonding interaction; E_A = adsorption energy per molecule; E_T = H-bonding and adsorption energy per unit area; E_{HA} = H-bonding energy per pmol of adsorbed molecules. At high concentrations, the assembly formation is directed by the total energy per unit area, *i.e.* E_T. In the latter case, the self-assembled network formed by molecule **2** is the most stable. When the number of molecules adsorbed is fixed to sub-monolayer coverage (low concentration regime), the expected assembly is that formed by the $[(\mathbf{1})_3{\cdot}(\mathbf{2})_2]_n$ network

Pattern	A/nm^2	Molecules/H-bonding interactions per unit cell	C_S/pmol cm^{-2}	E_H/eV[a]	E_A/eV[b]	E_T/eV nm^{-2}	E_{HA}/eV pmol^{-1}
1	1.4 ± 0.2	1/1	119	0.45 ± 0.06	0.85	0.93	$(2.7 \pm 0.3) \times 10^{11}$ (10 ± 1 kcal mol^{-1})
2	0.9 ± 0.1	2/3	369	0.44 ± 0.06	0.18	1.62	$(4.0 \pm 0.5) \times 10^{11}$ (15 ± 2 kcal mol^{-1})
$[(\mathbf{1})_3{\cdot}(\mathbf{2})_2]_n$	13.4 ± 0.6	3 (**1**) + 2 (**2**)/6	61	0.68 ± 0.06		0.52	$(4.9 \pm 0.4) \times 10^{11}$ (19 ± 2 kcal mol^{-1})[c]

[a] DFT calculated *in vacuo* interaction energies (ESI†). The uncertainties are the standard deviations of the melamine H-bond dimer DFT energies reported in ref. 10 and 11 and this work, corresponding to values of 0.34, 0.43 and 0.44 eV, respectively. [b] Parameterized with 0.061 eV for each sp^2 C present.[12] [c] The calculation is as follows: for each 3/5 pmol of molecule **1** and 2/5 pmol of molecule **2** there are 6/5 pmol of H-bond interactions worth 0.68 eV each (see ESI†).

used is equivalent (or lower) to that required to form a mixed monolayer of **1** and **2** on HOPG. Under such conditions, the driving force ruling the molecular packing is the gain in energy per mole of molecules in the adsorbed pattern: in fact, for sub-monolayer coverages, the packing energy density (eV nm^{-2}) does not determine the geometry of the physisorbed assembly. The adsorption energy of the individual components can be also ruled out (as long as it is $\gg$kT), since there is no competitive adsorption between the components. Table 1 reveals that the H-bonding energy of adsorbed molecules for the $[(\mathbf{1})_3{\cdot}(\mathbf{2})_2]_n$ pmol phase is higher than that for the mono-component phases, thus providing unambiguous explanation of the generation of such bicomponent assemblies. On the other hand, at high concentrations, the system tends to minimize its energy per unit area, leading to the formation of a patterned network composed of only molecule **2**. It is worth noting that the difference in H-bonding energy between a pmol of assembly **2** and that of the hybrid $[(\mathbf{1})_3{\cdot}(\mathbf{2})_2]_n$ is 0.9×10^{11} eV (3.6 kcal mol^{-1}). Thus, if the gain in energy from dipole–dipole, van der Waals or other isotropic interactions in pattern **2** is higher than the latter value, the $[(\mathbf{1})_3{\cdot}(\mathbf{2})_2]_n$ porous assembly is not the thermodynamically-favored phase. The upper limit in van der Waals interactions hindering the formation of porous networks was previously set to *ca.* 0.11 eV per molecule (2.5 kcal mol^{-1}) for a melamine and PTCDI pair,[8] *i.e.* lower than the 3.6 kcal mol^{-1} threshold value here determined.

In summary, H-bond recognition among melamine and a linear bis-uracilic module allows the formation of a porous bicomponent network at the solid–liquid interface. In analogy to self-assembly under UHV conditions, where the concentration conditions are used to direct polymorphism, we worked at sub-monolayer coverages to promote the formation of porous structures over tightly packed monolayers. Although other critical parameters such as solvent and isotropic molecular interactions should be taken into account to accurately pre-programme the formation of multi-component arrays, our simplified model offers reliable prediction of 2D crystal formation at the solid–liquid interface when predesigned molecular modules are employed.

This work was supported by the EU Marie-Curie RTN PRAIRIES (MRTN-CT-2006-035810) and EST–SUPER (MEST-CT-2004-008128), MIUR (Firb RBIN04HC3S), the Belgian National Research Foundation (FRS-FNRS, contract no. 2.4.625.08 F), the University of Namur, the ERA-Chemistry SurConFold project. ALP thanks Università di Trieste for the doctoral fellowship.

Notes and references

1 (*a*) G. R. Desiraju, *Angew. Chem., Int. Ed. Engl.*, 1995, **34**, 2311; (*b*) M. W. Hosseini, *Acc. Chem. Res.*, 2005, **38**, 313; (*c*) M. D. Hollingsworth, *Science*, 2002, **295**, 2410.
2 (*a*) S. De Feyter and F. C. De Schryver, *Chem. Soc. Rev.*, 2003, **32**, 139; (*b*) K. G. Nath, O. Ivasenko, J. A. Miwa, H. Dang, J. D. Wuest, A. Nanci, D. F. Perepichka and F. Rosei, *J. Am. Chem. Soc.*, 2006, **128**, 4212; (*c*) M. Surin, P. Samorí, A. Jouaiti, N. Kyritsakas and M. W. Hosseini, *Angew. Chem., Int. Ed.*, 2007, **46**, 245; (*d*) M. Surin and P. Samorí, *Small*, 2007, **3**, 190; (*e*) L. Piot, D. Bonifazi and P. Samori, *Adv. Funct. Mater.*, 2007, **17**, 3689.
3 (*a*) D. Bonifazi, H. Spillmann, A. Kiebele, M. de Wild, P. Seiler, F. Cheng, H.-J. Güntherodt, T. Jung and F. Diederich, *Angew. Chem., Int. Ed.*, 2004, **43**, 4759.
4 (*a*) J. V. Barth, *Annu. Rev. Phys. Chem.*, 2007, **58**, 375; (*b*) J. V. Barth, G. Costantini and K. Kern, *Nature*, 2005, **437**, 671.
5 P. Samorí, N. Severin, K. Müllen and J. P. Rabe, *Adv. Mater.*, 2000, **12**, 579.
6 (*a*) S. Lei, K. Tahara, F. C. De Schryver, M. V. d. Auweraer, Y. Tobe and S. De Feyter, *Angew. Chem., Int. Ed.*, 2008, **47**, 2964; (*b*) L. Kampschulte, T. L. Werblowsky, R. S. K. Kishore, M. Schmittel, W. M. Heckl and M. Lackinger, *J. Am. Chem. Soc.*, 2008, **130**, 8502.
7 (*a*) J. A. Zerkowski, C. T. Seto and G. M. Whitesides, *J. Am. Chem. Soc.*, 1992, **114**, 5473; (*b*) C. T. Seto and G. M. Whitesides, *J. Am. Chem. Soc.*, 1990, **112**, 6409; (*c*) M. Arduini, M. Crego-Calama, P. Timmerman and D. N. Reinhoudt, *J. Org. Chem.*, 2003, **68**, 1097; (*d*) S. Yagai, S. Mahesh, Y. Kikkawa, K. Unoike, T. Karatsu, A. Kitamura and A. Ajayaghosh, *Angew. Chem., Int. Ed.*, 2008, **47**, 4691.
8 (*a*) U. K. Weber, V. M. Burlakov, L. M. A. Perdigao, R. H. J. Fawcett, P. H. Beton, N. R. Champness, J. H. Jefferson, G. A. D. Briggs and D. G. Pettifor, *Phys. Rev. Lett.*, 2008, **100**, 156101; see also: (*b*) J. A. Theobald, N. S. Oxtoby, M. A. Phillips, N. R. Champness and P. H. Beton, *Nature*, 2003, **424**, 1029.
9 A. Llanes-Pallas, M. Matena, T. Jung, M. Prato, M. Stöhr and D. Bonifazi, *Angew. Chem., Int. Ed.*, 2008, DOI: 10.1002/anie.200802325.
10 W. Xu, M. Dong, H. Gersen, E. Rauls, S. Vázquez-Campos, M. Crego-Calama, D. N. Reinhoudt, I. Stensgaard, E. Laegsgaard, T. R. Linderoth and F. Besenbacher, *Small*, 2007, **3**, 854.
11 J. Ma, B. L. Rogers, M. J. Humphry, D. J. Ring, G. Goretzki, N. R. Champness and P. H. Beton, *J. Phys. Chem. B*, 2006, **110**, 12207.
12 R. Zacharia, H. Ulbricht and T. Hertel, *Phys. Rev. B*, 2004, **69**, 155406.